Renewable Energy-Based Micro-Grid for Clean Electricity and Green Hydrogen Production

Issa Zaiter[a], Ahmad Mayyas[b] and Raed Jaradat[c]
College of Engineering, Department of Management Science and Engineering, Khalifa University, Abu Dhabi, U.A.E.

Keywords: Sustainability, Energy System Modeling, Linear Programming Optimization, Power Generation, Hydrogen Production.

Abstract: The expected rise in hydrogen use offers a chance to speed up the decarbonization of the power generation sector. In this study, a linear programming optimization model is developed to determine the optimal technology capacity for a power and hydrogen production system driven by 100% renewable energy serving 25,000 capita with a total annual power demand of 532 GWh and an annual hydrogen demand of 5255 tons. The model aims to identify the optimal capacities of renewable energy sources and energy storage technologies to minimize system costs while meeting the demand for electricity and hydrogen. The results show the optimal system includes 59 MW of wind turbines, 630 MW of solar PV panels, 368 MW of polymer electrolyte membrane electrolyzer, 126 MW of proton exchange membrane fuel cells, 163 MW of lithium-ion batteries, and 111,000 m^3 of hydrogen storage. The total annualized system cost is $182 million, with electricity priced at $0.29 per kWh and green hydrogen at $5 per kg. By integrating hydrogen production with renewable energy-based power generation, It is concluded that a 100% renewable energy-driven system can meet the power and hydrogen demand for a sustainable community with the environmental benefit of zero carbon emissions, albeit with a higher price for a unit of power.

1 INTRODUCTION

Climate change and resource depletion are significant challenges to sustainable development, and renewable energy offers potential solutions. However, the intermittent nature of renewable energy sources emphasizes the need for reliable energy storage to ensure a consistent power supply. Energy storage ensures consistent power supply during demand fluctuations and is essential for managing surpluses as renewable energy is integrated into the grid (Rajeevkumar Urs et al., 2024). Hydrogen is gaining potential in industrial decarbonization (Zaiter et al., 2024). In addition, hydrogen-based storage systems, along with hybrid solutions combining hydrogen and batteries, offer promising long-term storage options for renewable energy. These technologies can help address energy storage challenges and reduce power variability in renewable systems (Zaiter et al., 2023), in addition to reducing the energy storage cost (Çağatay Iris and Lam, 2021).

The purpose of this study is to assess the feasibility of a 100% renewable energy-based system for microgrids and hydrogen production to meet the energy needs of a 25,000-person community. The study focuses on ensuring the community relies entirely on clean energy to satisfy demand across all sectors. The paper is structured as follows. Section 2 presents the problem statement and mathematical formulation, followed by Section 3 for results and discussion. Finally, Section 4 concludes the paper.

2 PROBLEM STATEMENT AND MATHEMATICAL FORMULATION

Two types of renewable power generation technologies: wind turbine power plants and solar photovoltaic power plants are assessed . It also incorporates two energy storage technologies into the system. The first is a lithium-ion battery (LIB) system. The second is a hydrogen system consisting of a polymer elec-

[a] https://orcid.org/0000-0001-7497-5773
[b] https://orcid.org/0000-0002-0367-6503
[c] https://orcid.org/0000-0002-1271-9202

Zaiter, I., Mayyas, A. and Jaradat, R.
Renewable Energy-Based Micro-Grid for Clean Electricity and Green Hydrogen Production.
DOI: 10.5220/0013138400003893

In *Proceedings of the 14th International Conference on Operations Research and Enterprise Systems (ICORES 2025)*, pages 239-245
ISBN: 978-989-758-732-0; ISSN: 2184-4372

trolyte membrane electrolyzer (PEMEC), a polymer electrolyte membrane fuel cell (PEMFC), a hydrogen compressor, and hydrogen storage.

Electricity demand is analyzed hourly based on a year's worth of historical data, showing peaks during the day. In the absence of historical data, an assumed hourly profile is used for hydrogen demand. A linear programming optimization model is developed to identify the optimal power generation capacity of each technology, allocate capacity for each energy storage technology, and outline the hourly energy storage dynamics, including charging and discharging patterns and energy levels for each storage technology.

The mathematical formulation, which includes the parameters used, the decision variables, the objective function, and the constraints of the model, is presented. For simplicity, an overview is also presented (Fig. 1). Eight technologies are indexed by i where $i \in [1,8]$, representing wind, solar, hydrogen electrolyzer, hydrogen storage, hydrogen fuel cell, battery charging capacity, battery discharging capacity, and battery storage capacity, respectively.

Parameters

N : Number of technologies $(N = 8)$
Z : Annualized system cost $(\$/\text{year})$
c_i : Capital cost of i $(\$/\text{kW})$ $(i = 1,\ldots,N)$
f_i : Fixed cost of i $(\$/\text{kW/year})$ $(i = 1,\ldots,N)$
v_i : Variable cost of i $(\$/\text{kWh})$ $(i = 1,\ldots,N)$
w_i : Capital recovery factor for i $(i = 1,\ldots,N)$
r : Project discount rate $(\%)$
n_i : Lifetime of technology i in years $(i = 1,\ldots,N)$
T : Total number of hours in the year $(T = 8760)$
h : Time step of one hour $(h = 1)$

Index

t : Number of hour in the year $t \in \{1,\ldots,T\}$

Decision Variables

The decision variables include each technology's installation capacity, hourly energy input/output, battery state of charge, and hydrogen storage level.

(i) *Variables based on technology capacity*:

X_i : Installation capacity of i in (kW) $\quad \forall i = 1,\ldots,N$

(ii) *Variables based on hourly energy input and output*:

Y_{it} : Energy flow (kWh) $\quad \forall i = 1,\ldots,N, \forall t = 1,\ldots,T$
B_t : Battery charge at hour t (kWh) $\quad \forall t = 1,\ldots,T$
H_t : Hydrogen level at hour t (kWh) $\quad \forall t = 1,\ldots,T$

Objective Function

The objective function is to minimize the total annualized costs of the system, as shown in Eq. (1), therefore the total cost of the system and the levelized cost of electricity. Total annualized system cost encompasses three key components: capital cost, fixed operational cost, and variable operational cost. The capital recovery factor ensures the system's capital cost is distributed evenly over its lifetime. Eq. (2) shows the capital recovery factor.

$$\text{Minimize } Z = \sum_{i=1}^{N} \left((w_i \cdot c_i + f_i) \cdot X_i + v_i \cdot \sum_{t=1}^{T} Y_{it} \right) \tag{1}$$

where

$$w_i = \frac{r \cdot (1+r)^{n_i}}{(1+r)^{n_i} - 1} \quad \forall i = 1,\ldots,N \tag{2}$$

Constraints

Five distinct sets of constraints (C1 to C5) represent various elements: wind power, solar power, hydrogen system (electrolyzer, storage, and fuel cell system), battery operation, and power demand. Additionally, a non-negativity constraint (C6) is imposed.

C1: Wind Power

A model, given in Eq. (3), is used for the calculation of wind power yield (Vargas et al., 2019).

$$Y_{1t} = \begin{cases} \frac{1}{2} \cdot \frac{\rho \cdot A_w}{P_w} \cdot e_w \cdot V_t^3 \cdot X_1 \cdot h & \text{if } Vi \le V_t \le Vo \\ 0 & \text{otherwise} \end{cases} \tag{3}$$

ρ : Air density (kg/m^3)
A_w : Swept area of the wind turbine blades (m^2)
e_w : Efficiency of the wind turbine $(\%)$
P_w : Rated power capacity of the wind turbine (W)
V_t : Average wind speed at hour t (m/s)
h : Height of the wind turbine (m)
Vi : Cut-in speed of the wind turbine (m/s)
Vo : Cut-off speed of the wind turbine (m/s)

C2: Solar Power

Eq. (4) estimates solar energy production, accounting for key variables influencing the power output (Pereira et al., 2024). It encompasses various factors,

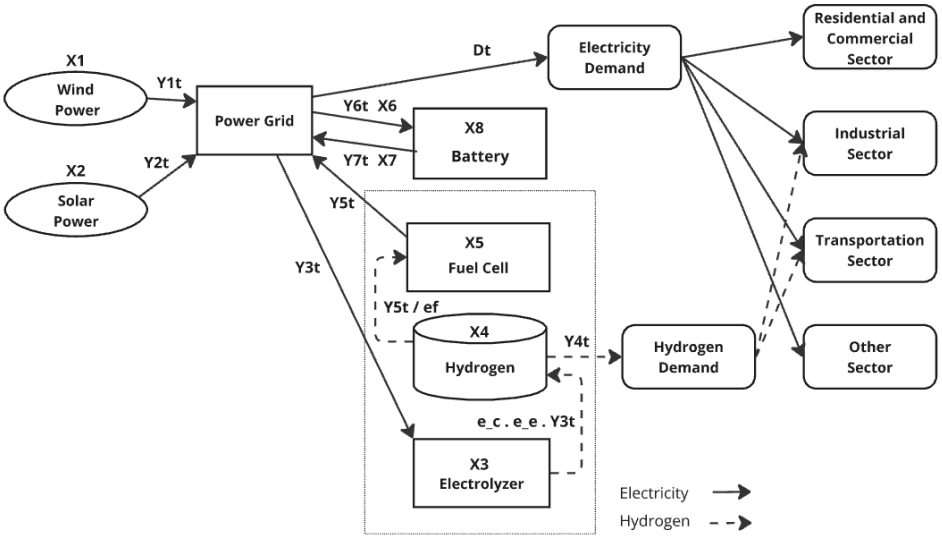

Figure 1: The model mathematical overview at a given time t.

such as solar panel area, nominal power rating, the efficiency of the photovoltaic panel, and the amount of direct normal irradiance.

$$Y_{2t} = \frac{A_s}{P_s} \cdot e_s \cdot \mathrm{I}_t \cdot X_2 \quad \forall t = 1, \ldots, T \tag{4}$$

A_s : Area of the PV panel (m^2)

P_s : Rated power capacity of the PV panel (W)

e_s : Efficiency of the PV panel $(\%)$

I_t : Average DNI at hour t $(\mathrm{Wh/m^2})$

C3: Hydrogen Electrolyzer, Storage, and Fuel Cell

Equation (5) illustrates the hydrogen storage level at the end of each hour (t). The electrolyzer and fuel cell belong to the proton exchange membrane (PEM) category. The hydrogen storage level at the beginning of the first hour (t_0) of the year is assumed to be 10% of the hydrogen storage capacity $(H_0 = 0.10X_4)$. The hydrogen storage level (kWh), which can be converted to kg using the higher hydrogen heating value of 39.39-kilowatt hours per kilogram, is determined by the sum of the accumulated hydrogen level of the preceding hour (H_{t-1}), and the amount of hydrogen produced by the electrolyzer —which is equal to the amount of energy that enters the electrolyzer multiplied by the efficiency of the electrolyzer and the efficiency of the hydrogen compressor $(e_c \cdot e_e \cdot Y_{3t})$—minus the hydrogen feeding the demand at a specific hour (Y_{4t}), and minus the hydrogen energy used in the fuel cell—which equals the power produced in the fuel cell divided by the efficiency of the fuel cell (Y_{5t}/e_f).

Equation (6) presents the constraint that ensures that the input power to the electrolyzer (Y_{3t}) at any hour (t) is less than or equal to the electrolyzer capacity (X_3). Similarly, Eq. (7) demonstrates the constraint that ensures that the hydrogen storage level (H_t) does not exceed the hydrogen storage capacity (X_4) at any hour (t). Lastly, Eq. (8) presents the constraint that ensures the amount of hydrogen entering the fuel cell (Y_{5t}/e_f) is always less than or equal to the fuel cell capacity (X_5).

$$\mathrm{H}_t = \mathrm{H}_{t-1} + e_c \cdot e_e \cdot Y_{3t} - Y_{4t} - \frac{Y_{5t}}{e_f}, \quad \forall t = 1, \ldots, T \tag{5}$$

$$Y_{3t} \leq X_3 \cdot h \quad \forall t = 1, \ldots, T \tag{6}$$

$$H_t \leq X_4 \cdot h \quad \forall t = 1, \ldots, T \tag{7}$$

$$\frac{Y_{5,t}}{e_f} \leq X_5 \cdot h \quad \forall t = 1, \ldots, T \tag{8}$$

e_e : Efficiency of the electrolyzer $(\%)$

e_c : Efficiency of the hydrogen compressor $(\%)$

e_f : Efficiency of the fuel cell $(\%)$

C4: Battery Operation

The model assumes LIBs for grid power storage. LIBs are favored in power storage applications for their high power and energy density (Kebede et al., 2022).

Equation (9) presents the battery state of charge (i.e., battery level) at the end of each hour (t). No carryover storage level from the previous hour is assumed, and therefore, the battery level at the beginning of the first hour of the year is zero $(B_0 = 0)$. The

battery level is composed of the sum of the battery level from a previous hour (B_{t-1}), plus the amount of energy entered the battery multiplied by the battery efficiency ($e_b.Y_{6t}$), minus any energy feeding the grid from the battery (Y_{7t}). All are multiplied by a $(1-f_d)$ factor to compensate for battery self-discharge.

Equation (10) presents the constraint that ensures that the energy out from the power grid and charging the battery (Y_{6t}) does not exceed the battery charging capacity (X_6). Similarly, Eq. (11) demonstrates the constraint that ensures the energy leaving the battery and feeding the power grid (Y_{7t}) does not exceed the battery discharging capacity (X_7).

Equation (12) correlates the battery charging capacity to the battery storage capacity using the battery C-rate factor, which measures how much the battery can charge/discharge relative to the battery's full capacity, expressed in C-number. For example, 2C means that the battery needs half an hour to charge fully, while 0.5C means that the battery needs two hours to charge fully.

Similarly, Eq. (13) presents the battery discharge capacity in terms of the battery storage capacity using the battery C-rate factor. In addition, Eq. (14) provides a constraint to ensure the battery level at any time t does not exceed the battery storage capacity multiplied by the maximum state of charge the battery is allowed to reach. Similarly, Eq. (15) ensures the battery level at any time will not drop below a certain level and, therefore, allow the battery to reach the maximum allowed depth of discharge only (Atieh et al., 2018).

$$\mathrm{B}_t = (1-f_b)\cdot(\mathrm{B}_{t-1} + e_b \cdot Y_{6t} - Y_{7t}) \quad \forall t = 1,\ldots,T \tag{9}$$

$$Y_{6t} \leq X_6 \cdot h \quad \forall t = 1,\ldots,T \tag{10}$$

$$Y_{7t} \leq X_7 \cdot h \quad \forall t = 1,\ldots,T \tag{11}$$

$$X_6 = f_c \cdot X_8 \tag{12}$$

$$X_7 = f_c \cdot X_8 \tag{13}$$

$$\mathrm{B}_t \leq f_{soc} \cdot X_8 \cdot h \quad \forall t = 1,\ldots,T \tag{14}$$

$$\mathrm{B}_t \geq (1-f_{dod}) \cdot X_8 \cdot h \quad \forall t = 1,\ldots,T \tag{15}$$

f_b : Battery self-discharge rate (% per hour)

e_b : Battery efficiency (%)

f_c : Battery C-rate

f_{soc} : Maximum state of charge battery (%)

f_{dod} : Maximum depth of discharge battery (%)

C5: Power Balance

The total power feeding the grid from various sources at every hour t —wind (Y_{1t}), solar (Y_{2t}), fuel cells (Y_{5t}), and batteries (Y_{7t})—must balance with the power to electricity demand (D_t), hydrogen electrolyzers (Y_{3t}), and batteries (Y_{6t}) as depicted in Eq. (16).

$$Y_{1t} + Y_{2t} + Y_{5t} + Y_{7t} = D_t + Y_{3t} + Y_{6t} \quad \forall t = 1,\ldots,T \tag{16}$$

C6: Non-negativity

Constraints (17-20) refer to the non-negativity of the decision variables.

$$X_i \geq 0 \quad \forall i = 1,\ldots,N \tag{17}$$

$$Y_{it} \geq 0 \quad \forall i = 1,\ldots,N \quad \forall t = 1,\ldots,T \tag{18}$$

$$H_t \geq 0 \quad \forall t = 1,\ldots,T \tag{19}$$

$$B_t \geq 0 \quad \forall t = 1,\ldots,T \tag{20}$$

3 RESULTS AND DISCUSSION

3.1 Implementation

The model is implemented in Python using Gurobi Optimizer version 12.0.0. And compiled on a Dell PC with 16.0 GB RAM and an 11th-gen Intel(R) Core(TM) processor.

Table (1) summarizes the specific coefficients integrated into the objective function, and it serves as a reference point, offering insights into the parameters and values crucial to calculating the objective function and, consequently, the decision-making process in the given context (Energy Inforamation Adminstration, 2022) (Cole et al., 2021).

Table 1: Coefficients employed in the objective function.

i	1	2	3	4	5	6	7	8
n_i	20	20	20	40	20	10	10	10
c_i	1718	1120	340	0.6	500	0	0	345
f_i	27.57	15.97	75.2	0.003	16	0	0	35
v_i	0	0	0.025	0	0.025	0	0	0.05

Vestas V150-4.2 MW wind turbine data is used for the specification (Vestas, 2023). For data on wind speed , and NASA/POWER CERES/MERRA2 native resolution hourly data is used from 01/01/2021 through 12/31/2021 for location in the United Arab Emirates (UAE): latitude 24.5387 longitude 54.4223, at 50 meters elevation (NASA Langley Research Center, 2023).

In addition, the DNI data at a location in the UAE is used: latitude 24.4682, longitude 54.3493 using an online open access tool (Global Solar Atlas, 2023). The solar panels' specifications are based on the Sharp PV panel ND-AH330 330 W poly-crystalline silicon photovoltaic modules.

The UAE's data hourly power consumption profile is utilized, accounting for fluctuations in electricity demand across various times of the day and throughout the year (Bayanat, 2023) with a total annual power demand of 532 GWh serving the 25,000 capita.

An annual demand for hydrogen of 5255 tons is considered (275 tons annually for the transportation sector to power 8,000 hydrogen fuel cell vehicles, each driving around 6875 km per year based on 200 km mileage per 1 kg of hydrogen, and 4980 tons annually for the industrial sector). While there is no specific hourly pattern for hydrogen consumption, a load profile assuming a fixed hourly demand throughout the year is generated.

The hydrogen storage is assumed to be pressurized vessels, with the assumed capital cost of 0.6 \$/kWh, equivalent to 20 \$/kg (based on the higher heating value of 39.39 kWh/kg of hydrogen) (Susan Schoenung, 2011). The hydrogen storage volume is determined based on the lower heating value of hydrogen and a hydrogen density of 14.94 kg/m^3, under 200 bar pressure and 15°C temperature. Table (2) presents the various parameter values used in the model.

Table 2: Coefficients employed in the constraints.

Parameter	Value	Unit
A_s	1.94	m^2
A_w	17671	m^2
e_b	90	%
e_c	85	%
e_e	73.5	%
e_f	55	%
e_s	17	%
e_w	35	%
f_b	0.0014	% per hour
f_c	1	-
f_{soc}	80	%
f_{dod}	80	%
J	5255	ton/year
K	532E6	kWh/year
p	5000	\$/ton
P_s	330	W
P_w	4E6	W
r	7	%
m	1.225	kg/m^3
Vi	3	m/s
Vo	22.5	m/s

To enhance our understanding of the economic dynamics within the system, the levelized cost of electricity (LCOE) is calculated using the simple fixed charge rate method. To determine the LCOE, the revenue of selling the produced hydrogen is subtracted from the total annualized system cost and divide it by the total produced power in a year, as illustrated in Eq. (21).

$$LCOE = \frac{Z - p \cdot J}{K} \tag{21}$$

where

p : Selling price of hydrogen (\$/ton)
J : Total amount of hydrogen demand (ton/year)
K : Total amount of power demand (kWh/year)

3.2 Numerical Results

The results (Fig. 2) illustrate the hourly profiles of power generation and storage technologies over a weekly scale; it provides detailed insight into energy supply and storage dynamics.

The solar power plant's output aligns with the direct normal irradiance profile. The results illustrate how hydrogen production in the electrolyzer fluctuates inversely to match daily and seasonal power demand variations. During high-demand periods, such as the summer season, hydrogen production decreases due to increased electricity use for cooling. The output of hydrogen feedstock remains consistent in fulfilling hourly demand year-round.

The graphical representation illustrates the hourly hydrogen storage level (Fig. 3) as a percentage of its full capacity, showcasing the buffering capacity that hydrogen can contribute to the overall system design.

The optimization problem results indicate that meeting the annual power requirement of a community of 25,000 people—totaling 532 GWh—and a hydrogen demand of 5,255 tons can be achieved with a fully renewable energy system. This system would consist of 15 wind turbines, each with a 4 MW capacity, and approximately 1.9 million solar PV panels, each rated at 330 W. Additionally, it would require 368 MW polymer electrolyte membrane electrolyzer, 126 MW proton exchange membrane fuel cells, 163 MW lithium-ion batteries, and 111,000 m^3 hydrogen storage. The projected annualized system cost for this setup is \$182 million, with a levelized cost of electricity (LCOE) of \$0.29 per kWh, based on a hydrogen price of \$5,000 per ton.

4 CONCLUSION

In conclusion, the integration of a hybrid Micro-Grid system with hydrogen production, powered entirely by renewable energy sources, presents a viable pathway for advancing the decarbonization of the power

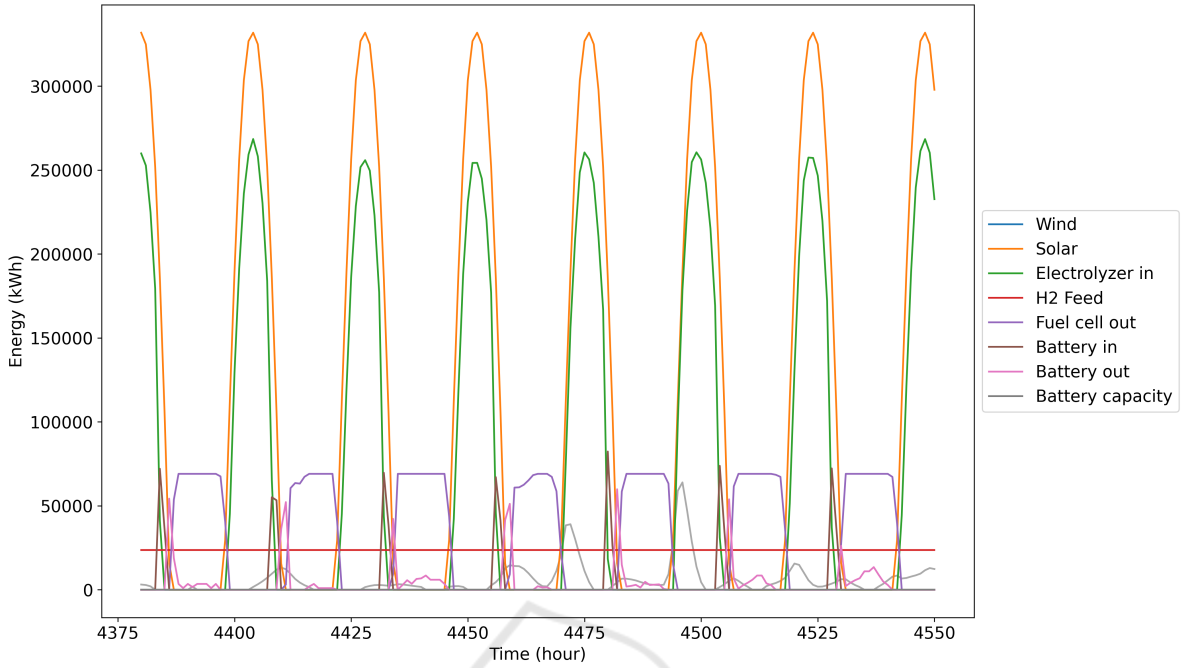

Figure 2: Hourly profile over the first week of July.

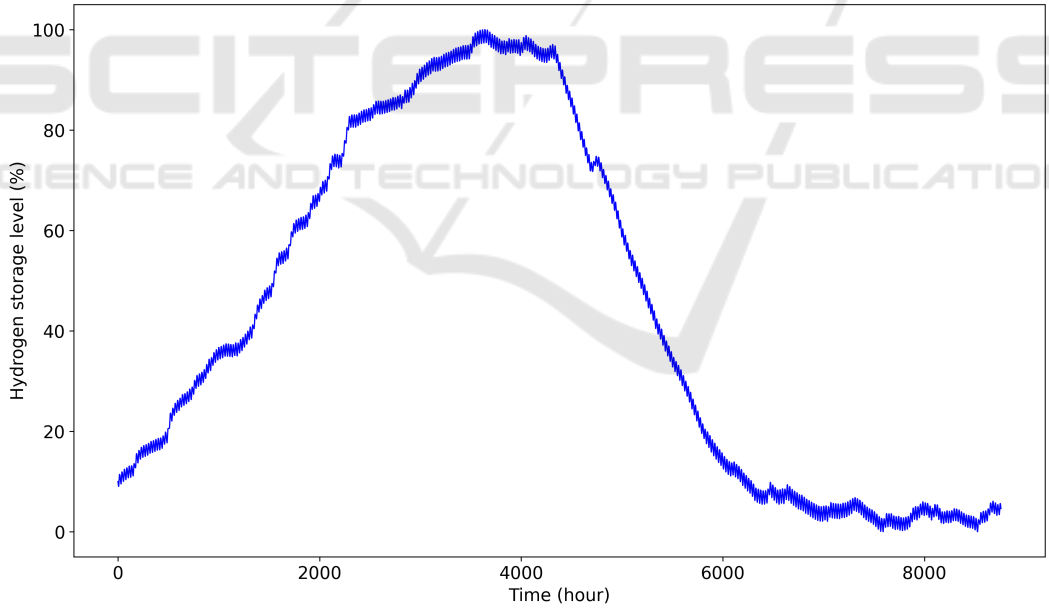

Figure 3: Hourly hydrogen storage level over a full year (% of full capacity).

generation sector. A linear programming optimization model is used to identify the optimal capacities for wind turbines, solar PV panels, electrolyzers, fuel cells, batteries, and hydrogen storage necessary to meet the energy and hydrogen demands of a community of 25,000 people. The results demonstrate that a system featuring 59 MW of wind turbines, 630 MW of solar PV panels, 368 MW of polymer electrolyte membrane electrolyzer, 126 MW of proton exchange membrane fuel cells, 163 MW of lithium-ion batteries, and 111,000 m^3 of hydrogen storage can fulfill the annual requirements of 532 GWh of electricity and 5,255 tons of hydrogen, with a total annualized system cost of $182 million.

The findings underscore the benefits of such a system, including the efficient use of surplus renewable energy and minimized energy losses due to power curtailment. The detailed hourly profiles of power generation, storage levels, and hydrogen production illustrate the system's flexibility and its ability to adapt to varying energy demands throughout the year. During periods of high electricity demand, particularly in summer, the system effectively balances energy storage and hydrogen production, maintaining a consistent supply of hydrogen while managing electricity needs.

Overall, this study confirms that a fully renewable energy system incorporating hydrogen production and storage is not only feasible but also cost-effective. By leveraging renewable resources and advanced storage technologies, this system can significantly contribute to the transition towards a low-carbon energy future, providing a reliable and sustainable energy solution for communities.

REFERENCES

Atieh, A., Charfi, S., and Chaabene, M. (2018). Chapter 8 - hybrid pv/batteries bank/diesel generator solar-renewable energy system design, energy management, and economics. In Yahyaoui, I., editor, *Advances in Renewable Energies and Power Technologies*, pages 257–294. Elsevier.

Bayanat (2023). UAE Open Data Portal. https://bayanat.ae/en. Accessed on February 21, 2024.

Cole, W., Frazier, A. W., and Augustine, C. (2021). Cost projections for utility-scale battery storage: 2021 update. Technical Report NREL/TP-6A20-79236, National Renewable Energy Laboratory, Golden, CO.

Energy Inforamation Adminstration (2022). Annual energy outlook 2022 - assumptions. https://www.eia.gov/outlooks/aeo/assumptions/pdf/table_8.2.pdf. Accessed on February 21, 2024.

Global Solar Atlas (2023). Interactive map for solar and photovoltaic potential. https://globalsolaratlas.info/map?s=24.468231,54.349365,10&c=23.870769,50.603027,7. Accessed on February 21, 2024.

Kebede, A. A., Kalogiannis, T., Van Mierlo, J., and Berecibar, M. (2022). A comprehensive review of stationary energy storage devices for large scale renewable energy sources grid integration. *Renewable and Sustainable Energy Reviews*, 159:112213.

NASA Langley Research Center (2023). Nasa power. https://power.larc.nasa.gov/. Accessed on February 21, 2024.

Pereira, S., Canhoto, P., and Salgado, R. (2024). Development and assessment of artificial neural network models for direct normal solar irradiance forecasting using operational numerical weather prediction data. *Energy and AI*, 15:100314.

Rajeevkumar Urs, R., Mussawar, O., Zaiter, I., Mezher, T., and Mayyas, A. (2024). Navigating the cost-efficiency frontier: Exploring the viability of grid-connected energy storage systems in meeting district load demand. *Energy Conversion and Management*, 299:117828.

Susan Schoenung, P. (2011). Economic analysis of large-scale hydrogen storage for renewable utility applications. Unlimited Release SAND2011-4845, Longitude 122 West, Inc., Livermore, CA. 94551-0969. Contract #1024882.

Vargas, S. A., Esteves, G. R. T., Maçaira, P. M., Bastos, B. Q., Cyrino Oliveira, F. L., and Souza, R. C. (2019). Wind power generation: A review and a research agenda. *Journal of Cleaner Production*, 218:850–870.

Vestas (2023). Vestas v150-4.2 mw. https://www.vestas.com/en/products/4-mw-platform/V150-4-2-MW. Accessed on February 21, 2024.

Zaiter, I., Ramadan, M., Bouabid, A., El-Fadel, M., and Mezher, T. (2023). Potential utilization of hydrogen in the uae's industrial sector. *Energy*, 280:128108.

Zaiter, I., Ramadan, M., Bouabid, A., Mayyas, A., El-Fadel, M., and Mezher, T. (2024). Enabling industrial decarbonization: Framework for hydrogen integration in the industrial energy systems. *Renewable and Sustainable Energy Reviews*, 203:114782.

Çağatay Iris and Lam, J. S. L. (2021). Optimal energy management and operations planning in seaports with smart grid while harnessing renewable energy under uncertainty. *Omega*, 103:102445.